Vol 18 No 6, June 2009
1674-1056/2009/18(06)/2340-12

Chinese Physics B

© 2009 Chin. Phys. Soc.
and IOP Publishing Ltd

Phase dispersion of Raman and Rayleigh-enhanced four-wave mixings in femtosecond polarization beats*

Zhao Yan(赵 燕)[a], Nie Zhi-Qiang(聂志强)[a], Li Chang-Biao(李昌彪)[a], Zhang Yan-Peng(张彦鹏)[a]†, Gan Chen-Li(甘琛利)[a], Zheng Huai-Bin(郑淮斌)[a], Li Yuan-Yuan(李院院)[a], and Lu Ke-Qing(卢克清)[b]

[a] *Key Laboratory for Physical Electronics and Devices of the Ministry of Education, Xi'an Jiaotong University, Xi'an* 710049, *China*

[b] *State Key Laboratory of Transient Optics and Technology, Xi'an Institute of Optics and Precision Mechanics, Chinese Academy of Sciences, Xi'an* 710068, *China*

(Received 26 August 2008; revised manuscript received 24 October 2008)

Based on color-locking noisy field correlation in three Markovian stochastic models, phase dispersions of the Raman- and Rayleigh-enhanced four-wave mixing (FWM) have been investigated. The phase dispersions are modified by both linewidth and time delay for negative time delay, but only by linewidth for positive time delay. Moreover, the results under narrowband condition are close to the nonmodified nonlinear dispersion and absorption of the material. Homodyne and heterodyne detections of the Raman, the Rayleigh and the mixing femtosecond difference-frequency polarization beats have also been investigated, separately.

Keywords: phase dispersion, Raman, Rayleigh, four-wave mixing
PACC: 4265, 4250

1. Introduction

Lasers are inherent noisy devices, in which both the phase and amplitude of the field can fluctuate. Noisy light can be used to probe atomic and molecular dynamics, and it offers a unique alternative for the more conventional frequency domain spectroscopies and ultrashort pulse time domain spectroscopies. The color locking noisy light method is an intermediate between cw and short-pulse methods.[1−6]

Four-wave mixing (FWM) is a third-order nonlinear optical process.[7−10] Using femtosecond time-resolved FWM, valuable information on the dephasing dynamics in semiconductors and molecular materials has been obtained. The time resolution of this method is limited by the pulse width. However, the ultrafast dephasing phenomena can also be studied by time-delayed FWM with incoherent light. This technique is intrinsically related to the optical coherent transient spectroscopy with an advantage that the time resolution is determined by the correlation time τ_c of the color locking noisy light source. Since the relaxation time is deduced from the FWM spectrum, the measurement is not limited by the laser pulse width or the laser correlation time.[2−4]

Coherent Raman spectroscopy (CRS) is a powerful tool for studying the vibrational or rotational mode of a molecule. In Raman-enhanced FWM (one of the CRS techniques),[2,3,5] the Raman vibration is excited by the resonant excitation.[2] In contrast, Rayleigh-enhanced FWM[3,5] is a non-resonant process. The Raman- or Rayleigh-enhanced FWM may be superior to all other CRS techniques.[2,3,5] They possess the features of non-resonant background suppression, excellent spatial signal resolution, free choice of interaction volume and simple optical alignment. Moreover, phase matching can be achieved for a very wide frequency range from many hundreds to thousands of cm^{-1}.

Polarization beat between two excitation pathways is related to recent studies on quantum interference.[2−4,11,12] DeBeer *et al*[6] first performed the 980-as sum-frequency ultrafast modulation spec-

*Project supported by the National Natural Science Foundation of China (Grant No 60678005), the Foundation for the Author of National Excellent Doctoral Dissertation of China (Grant No 200339), the For Ying-Tong Education Foundation for Young Teachers in the Institutions of Higher Education of China (Grant No 101061) and the Specialized Research Fund for the Doctoral Program of Higher Education of China (Grant No 20050398017).

†Corresponding author. E-mail: ypzhang@mail.xjtu.edu.cn

troscopy (UMS) experiment. The Raman- and Rayleigh-enhanced polarization beats are an interesting way to study the stochastic properties of light.[2,3]

In this paper, based on the field-correlation of color-locking twin noisy lights, we have investigated the phase dispersions of the Raman- and Rayleigh-enhanced FWM. The phase dispersions are modified by both linewidth and time delay for negative time delay, but only by linewidth for positive time delay. The results under the narrowband condition are close to the nonmodified nonlinear dispersion and absorption of the material. Moreover, homodyne and heterodyne detections of the Raman, the Rayleigh and the mixing femtosecond difference-frequency polarization beat (FDPB) have also been exhibited. From the heterodyne detected FDPB, we can obtain the characteristics of the dispersion and absorption for the resonant Raman- and Rayleigh-enhanced FWM. Investigations of the phase dispersion of Raman and Rayleigh-enhanced FWM will help us to understand and optimize the nonlinear susceptibilities and the generated high-order nonlinear optical signals, which have potential applications in achieving better nonlinear optical materials and opt-electronic devices.

2. Basic theory

The Raman and Rayleigh femtosecond difference-frequency polarization beats (FDPB's) are the third-order nonlinear polarization beat phenomenon. Here the polarization beat is based on the interference at the detector between two FWM signals which originate from macroscopic polarizations excited simultaneously in the homogeneous or inhomogeneous broadening sample. It requires that all the polarizations have the same frequency.

The basic geometry is shown in Fig.1. Twin beams 1 and 2 consist of two frequency components ω_1 and ω_2, a small angle exists between them. Beam 3 with frequency ω_3 is almost propagating along the opposite direction of beam 1. Twin composite stochastic fields of beam 1, $E_{p1}(\boldsymbol{r},t)$, and beam 2, $E_{p2}(\boldsymbol{r},t)$, for homodyne detection scheme, can be written as

$$\begin{aligned} E_{p1} &= E_1(\boldsymbol{r},t) + E_2(\boldsymbol{r},t) \\ &= A_1(\boldsymbol{r},t)\exp(-\mathrm{i}\omega_1 t) + A_2(\boldsymbol{r},t)\exp(-\mathrm{i}\omega_2 t) \\ &= \varepsilon_1 u_1(t)\exp[\mathrm{i}(\boldsymbol{k}_1\cdot\boldsymbol{r}-\omega_1 t)] \\ &\quad + \varepsilon_2 u_2(t)\exp[\mathrm{i}(\boldsymbol{k}_2\cdot\boldsymbol{r}-\omega_2 t)], \\ E_{p2} &= E_1'(\boldsymbol{r},t) + E_2'(\boldsymbol{r},t) \\ &= A_1'(\boldsymbol{r},t)\exp[-\mathrm{i}\omega_1(t-\tau)] \\ &\quad + A_2'(\boldsymbol{r},t)\exp[-\mathrm{i}\omega_2(t-\tau)] \\ &= \varepsilon_1' u_1(t-\tau)\exp[\mathrm{i}(\boldsymbol{k}_1'\cdot\boldsymbol{r}-\omega_1 t+\omega_1\tau)] \\ &\quad + \varepsilon_2' u_2(t-\tau)\exp[\mathrm{i}(\boldsymbol{k}_2'\cdot\boldsymbol{r}-\omega_2 t+\omega_2\tau)]. \quad (1) \end{aligned}$$

Here, ε_i, $\boldsymbol{k}_i$ (ε_i', $\boldsymbol{k}_i'$) are the constant field amplitude and the wave vector of the ω_i component in beams 1 and 2, respectively; $u_i(t)$ is a dimensionless statistical factor that contains phase and amplitude fluctuations. It is taken to be a complex ergodic stochastic function of t, which obeys complex circular Gaussian statistics in chaotic field. And τ is a variable relative time delay between the prompt (unprimed) and delayed (primed) fields. To accomplish this the frequency-component ω_1 and ω_2 lights are split and recombined to provide two double-frequency pulses in such a way that the ω_1 and ω_2 components are delayed by τ in beam 2 (Fig.1), which is quite different from that of attosecond sum-frequency polarization beats.[2−4,6] On the other hand, the complex electric fields of beam 3 can be written as $E_3(\boldsymbol{r},t) = A_3(\boldsymbol{r},t)\exp(-\mathrm{i}\omega_3 t) = \varepsilon_3 u_3(t)\exp[\mathrm{i}(\boldsymbol{k}_3\cdot\boldsymbol{r}-\omega_3 t)]$. Here, ω_3, ε_3, and $\boldsymbol{k}_3$ are the frequency, the field amplitude and the wave vector of the field, respectively.

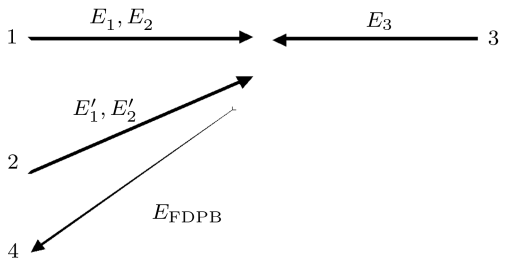


Fig.1. Phase-conjugation geometry of the Raman and Rayleigh FDPBs.

In an absorbing medium, the nonlinear interaction of beams 1 and 2 with the medium gives rise to the molecular-reorientation gratings and the thermal gratings, i.e., $\omega_{1,2}$ will induce their own non-resonant static molecular-reorientation gratings $G_{M1,2}$ and thermal gratings $G_{T1,2}$. The FWM signals are the results of the diffraction of beam 3 by these four gratings. The order parameters Q_{M1}, Q_{T1}, Q_{M2} and Q_{T2} of the four non-resonant static gratings satisfy the following equations:[2,3,5]

$$\begin{aligned} &\mathrm{d}Q_{M1}/\mathrm{d}t + \gamma_M Q_{M1} = \chi_M\gamma_M E_1(\boldsymbol{r},t)[E_1'(\boldsymbol{r},t)]^*, \\ &\mathrm{d}Q_{T1}/\mathrm{d}t + \gamma_T Q_{T1} = \chi_T\gamma_T E_1(\boldsymbol{r},t)[E_1'(\boldsymbol{r},t)]^*, \end{aligned}$$

$$\mathrm{d}Q_{M2}/\mathrm{d}t + \gamma_M Q_{M2} = \chi_M \gamma_M E_2'(\boldsymbol{r},t)[E_2(\boldsymbol{r},t)]^*,$$
$$\mathrm{d}Q_{T2}/\mathrm{d}t + \gamma_T Q_{T2} = \chi_T \gamma_T E_2'(\boldsymbol{r},t)[E_2(\boldsymbol{r},t)]^*. \quad (2)$$

Here $\gamma_{M,T}$ and $\chi_{M,T}$ are the relaxation rate and the nonlinear susceptibility of the molecular-reorientation grating and thermal grating, respectively.

On the one hand when the frequency difference $\Delta_1 = \omega_3 - \omega_1$ is much smaller than $\Delta_1' = \omega_3 - \omega_2$ (i.e., $\Delta_1 \ll \Delta_1'$ and $\Delta_1 \approx 0$) , the two resonant moving gratings, G_{RM} and G_{RT} with a large angle formed by the interference between the ω_1 frequency component of beam 2 and the ω_3 frequency component of beam 3, will excite the Rayleigh mode of the medium and enhance the FWM signals (i.e., Rayleigh-enhanced FWM). On the other hand, if only the frequency detuning $\Delta_2 = \Delta_1' - \Omega_R$ is near zero, the one large resonant moving grating, G_R formed by the interference between the ω_2 frequency component of beam 2 and the ω_3 frequency component of beam 3, will excite the Raman mode of the medium and enhance the FWM signals (i.e., Raman-enhanced FWM). The order parameters Q_R, Q_{RT} and Q_{RM} should satisfy the following equations:

$$\mathrm{d}Q_R/\mathrm{d}t + (\gamma_R - \mathrm{i}\Delta_2)Q_R = \chi_R \gamma_R [E_2(\boldsymbol{r},t)]^* E_3(\boldsymbol{r},t),$$
$$\mathrm{d}Q_{RM}/\mathrm{d}t + \gamma_M Q_{RM} = \chi_M \gamma_M [E_1'(\boldsymbol{r},t)]^* E_3(\boldsymbol{r},t),$$
$$\mathrm{d}Q_{RT}/\mathrm{d}t + \gamma_T Q_{RT} = \chi_T \gamma_T [E_1'(\boldsymbol{r},t)]^* E_3(\boldsymbol{r},t). \quad (3)$$

Based on Eqs.(2) and (3), the induced seven third-order nonlinear polarizations responsible for the FWM signals are

$$P_{M1} = Q_{M1}(\boldsymbol{r},t)E_3(\boldsymbol{r},t) = \chi_M \gamma_M S_1(\boldsymbol{r}) \int_0^\infty A_1(t-t')A_1^*(t-t'-\tau)A_3(t)\exp(-\gamma_M t')\mathrm{d}t', \quad (4)$$

$$P_{T1} = Q_{T1}(\boldsymbol{r},t)E_3(\boldsymbol{r},t) = \chi_T \gamma_T S_1(\boldsymbol{r}) \int_0^\infty A_1(t-t')A_1^*(t-t'-\tau)A_3(t)\exp(-\gamma_T t')\mathrm{d}t', \quad (5)$$

$$P_{M2} = Q_{M2}(\boldsymbol{r},t)E_3(\boldsymbol{r},t) = \chi_M \gamma_M S_2(\boldsymbol{r}) \int_0^\infty A_2^*(t-t')A_2(t-t'-\tau)A_3(t)\exp(-\gamma_M t')\mathrm{d}t', \quad (6)$$

$$P_{T2} = Q_{T2}(\boldsymbol{r},t)E_3(\boldsymbol{r},t) = \chi_T \gamma_T S_2(\boldsymbol{r}) \int_0^\infty A_2^*(t-t')A_2(t-t'-\tau)A_3(t)\exp(-\gamma_T t')\mathrm{d}t', \quad (7)$$

$$P_R = Q_R(\boldsymbol{r},t)E_2'(\boldsymbol{r},t) = \mathrm{i}\chi_R \gamma_R S_2(\boldsymbol{r}) \int_0^\infty A_2^*(t-t')A_3(t-t')A_2(t-\tau)\exp[-(\gamma_R - \mathrm{i}\Delta_2)t']\mathrm{d}t', \quad (8)$$

$$P_{RM} = Q_{M1}(\boldsymbol{r},t)E_1(\boldsymbol{r},t) = \chi_M \gamma_M S_1(\boldsymbol{r}) \int_0^\infty A_1^*(t-t'-\tau)A_3(t-t')A_1(t)\exp[-(\gamma_M - \mathrm{i}\Delta_1)t']\mathrm{d}t', \quad (9)$$

$$P_{RT} = Q_{T1}(\boldsymbol{r},t)E_1(\boldsymbol{r},t) = \chi_T \gamma_T S_1(\boldsymbol{r}) \int_0^\infty A_1^*(t-t'-\tau)A_3(t-t')A_1(t)\exp[-(\gamma_T - \mathrm{i}\Delta_1)t']\mathrm{d}t'. \quad (10)$$

Here $S_1(\boldsymbol{r}) = \exp\{\mathrm{i}[(\boldsymbol{k}_1 - \boldsymbol{k}_1' + \boldsymbol{k}_3)\cdot\boldsymbol{r} - \omega_3 t - \omega_1\tau]\}$ and $S_2(\boldsymbol{r}) = \exp\{\mathrm{i}[(\boldsymbol{k}_2' - \boldsymbol{k}_2 + \boldsymbol{k}_3)\cdot\boldsymbol{r} - \omega_3 t - \omega_2\tau]\}$. It can be appreciated that polarizations $P_C = P_{M2} + P_{T2}$ and $P_A = P_{M2} + P_{T2} + P_R$ correspond to an FWM process and a Raman-enhanced FWM process under the phase-matching condition $\boldsymbol{k}_2' - \boldsymbol{k}_2 + \boldsymbol{k}_3$, while $P_D = P_{M1} + P_{T1}$ and $P_B = P_{M1} + P_{T1} + P_{RM} + P_{RT}$ correspond to the other FWM process and the Rayleigh-enhanced FWM process under the phase-matching condition $\boldsymbol{k}_1 - \boldsymbol{k}_1' + \boldsymbol{k}_3$. The Raman- (Rayleigh-) enhanced FWM signal is proportional to the average of the absolute square of P_A (P_B) over the random variable of the stochastic process $\langle|P_A|^2\rangle$ ($\langle|P_B|^2\rangle$), which involves fourth- and second-order coherence function of $u_i(t)$. All these FWM signals have the same frequency, i.e., ω_3. As a result, FDPB originates from the interference between the macroscopic polarizations from the Rayleigh-enhanced FWM and the Raman-enhanced FWM signals. The beat signal (beam 4) is along the opposite direction of beam 2 approximately.[2,3,5] In this paper three Markovian noise models, the chaotic field model (CFM), the phase-diffusion model (PDM) and the Gaussian-amplitude model (GAM) are considered at the intensity level to fully appreciate the subtle features of FWM spectroscopy.[2,3,5]

3. Homodyne detection of FDPB

The FDPB signal is proportional to the average of the absolute square of $P^{(3)}$ over the random variable of the stochastic process, so that the signal $I(\Delta_i,\tau) \propto \langle P^{(3)}(P^{(3)})^*\rangle$ contains different terms in the fourth- and second-order coherence functions of $u_i(t)$ in phase conjugation geometry. In general, the FDPB of homodyne detection (at the intensity level) can be viewed as the sum of three contributions: (i) the τ-independent or dependent auto-correlation terms of ω_1 component, which include $u_1(t)$ fourth-order and $u_3(t)$ second-order Markovian stochastic correlation functions; (ii) the τ-independent or dependent auto-correlation terms of ω_2 component, which include $u_2(t)$ fourth-order and $u_3(t)$ second-order Markovian stochastic correlation functions; (iii) the τ-dependent cross-correlation terms between ω_1 and ω_2 components, which include $u_1(t)$, $u_2(t)$ and $u_3(t)$ second-order Markovian stochastic correlation functions. Different Markovian stochastic models of the laser field only affect the fourth-, not second-order correlation functions.[2,3,5]

3.1. Raman FDPB

For the Raman FDPB, we have the total third-order polarization $P^{(3)} = P_A + P_D = (P_{M2} + P_{T2} + P_R) + (P_{M1} + P_{T1})$. Therefore, the homodyne-detection signal $I(\Delta_2,\tau)$ contains $5\times 5 = 25$ different terms which include the non-resonant terms of the ω_1 molecular-reorientation and thermal gratings, terms of the ω_2 molecular-reorientation and thermal gratings and Raman resonant mode, and the cross-correlation terms between FWM and Raman-enhanced FWM.

After performing the tedious integration from Eqs.(4)–(10), in the limit $\gamma_M, \gamma_R \gg \alpha_1,\ \alpha_2,\ \alpha_3 \gg \gamma_T$ we obtain

$$
\begin{aligned}
&I_{\mathrm{FDPB}}(\Delta_2,\tau)\\
&\propto \eta^2 \exp(-2\mathrm{i}\boldsymbol{\Delta k}\cdot\boldsymbol{r})\,\{[1+n_4\exp(-2\alpha_2|\tau|)]\,L_5 + L_6\}\\
&\quad + \{[1+n_4\exp(-2\alpha_1|\tau|)]\ \chi_M^2 + L_7\}\\
&\quad + \eta L_8\{\exp[\mathrm{i}\boldsymbol{\Delta k}\cdot\boldsymbol{r} - \mathrm{i}(\omega_1-\omega_2)|\tau|]\chi_A^*\\
&\quad + \exp[-\mathrm{i}\boldsymbol{\Delta k}\cdot\boldsymbol{r} + \mathrm{i}(\omega_1-\omega_2)|\tau|]\chi_A\}. \qquad (11)
\end{aligned}
$$

Here

$$
\begin{aligned}
L_5 &= \chi_M^2 - 2\gamma_R\Delta_2\chi_M\chi_R/(\gamma_R^2+\Delta_2^2)\\
&\quad +\gamma_R^2\chi_R^2/(\gamma_R^2+\Delta_2^2),\\
L_6 &= \exp(-2\alpha_2|\tau|)[2\chi_M\chi_T\\
&\quad - 2\gamma_R\Delta_2\chi_T\chi_R/(\gamma_R^2+\Delta_2^2) + \chi_T^2],\\
L_7 &= \exp(-2\alpha_1|\tau|)(2\chi_M\chi_T + \chi_T^2),\\
L_8 &= (\chi_M+\chi_T)\exp[-(\alpha_1+\alpha_2)|\tau|],\\
\chi_A &= \chi_M + \chi_T - \chi_R\gamma_R/(\Delta_2 + \mathrm{i}\gamma_R),\\
\eta &= \varepsilon_2'(\varepsilon_2)^*/\varepsilon_1(\varepsilon_1')^*,\\
\boldsymbol{\Delta k} &= (\boldsymbol{k}_1 - \boldsymbol{k}_1') - (\boldsymbol{k}_2' - \boldsymbol{k}_2),
\end{aligned}
$$

and n_4 equals 1, 0, 2 for the CFM, PDM and GAM, respectively.

First for CFM, the Raman FDPB versus τ shows the femtosecond scale modulation with a different frequency $\omega_1-\omega_2$ and damping rates α_1 and α_2. The constant term $\gamma_R^2\chi_R^2/(\gamma_R^2+\Delta_2^2)$ in Eq.(11), which is independent of the relative time-delay between twin beams 1 and 2, originates from the phase fluctuation of the chaotic fields, while the purely decay terms including the factors $\exp(-2\alpha_1|\tau|)$, $\exp(-2\alpha_2|\tau|)$ come from the amplitude fluctuation of the chaotic fields.

Secondly, for PDM the temporal behavior of the beat signal only reflects the characteristic of the lasers. The result is remarkably different from that based on the chaotic model. It is short of the purely auto-correlation decay terms including the factors $\exp(-2\alpha_1|\tau|)$ and $\exp(-2\alpha_2|\tau|)$, which are shown to be particularly insensitive to the phase fluctuation of the Markovian stochastic light fields. The drastic difference of the results also exists in the higher-order correlation in Rayleigh FDPB when the three Markovian stochastic models are employed.[2,3]

Thirdly, for GAM, in contrast to CFM and PDM, the decay term includes the factors $2\exp(-2\alpha_1|\tau|)$ and $2\exp(-2\alpha_2|\tau|)$. The τ-dependent term of Gaussian-amplitude field is larger than that of the chaotic field or the phase-diffusion field (see Fig.2), which originates from the amplitude fluctuation of the Markovian stochastic field. For this the physical explanation is that the Gaussian-amplitude field undergoes stronger intensity fluctuations than a chaotic field. On the other hand, the intensity (amplitude) fluctuations of the Gaussian-amplitude field or the chaotic field are always much larger than the pure phase fluctuations of the phase-diffusion field.

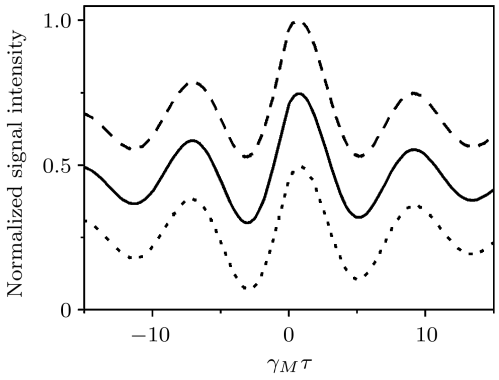


Fig.2. Raman FDPB signal intensity versus $\gamma_M\tau$ for $\chi_M/\chi_R = 0.5$, $\gamma_M/\gamma_R = 0.001$, $\chi_T/\chi_R = 0.5$, $\gamma_T/\gamma_M = 50$, $\alpha_2/\gamma_M = 0.1$, $\alpha_1/\gamma_M = \alpha_3/\gamma_M = 0.1$, $\Delta_2 = 0$, $r = 0$, $\omega_1/\alpha_1 = 127450$, $\omega_2/\alpha_1 = 119924$ and $\eta = 1$. The three curves represent the signal intensities for CFM (solid curve), GAM (dashed curve), and PDM (dotted curve).

3.2. Rayleigh FDPB

For the Rayleigh FDPB, we have the total third-order polarization $P^{(3)} = P_B + P_C = (P_{M1} + P_{RM} + P_{T1} + P_{RT}) + (P_{M2} + P_{T2})$. Therefore, the homodyne-detection signal $I(\Delta_1, \tau)$ contains $6 \times 6 = 36$ different terms which include the non-resonant terms of the ω_2 molecular-reorientation and thermal gratings, terms of the ω_1 molecular-reorientation and thermal gratings and Rayleigh resonant mode, and the cross-correlation terms between FWM and Rayleigh-enhanced FWM.

After performing the tedious integration of Eqs.(4)–(10), in the limit $\gamma_M, \gamma_R \gg \alpha_1, \alpha_2, \alpha_3 \gg \gamma_T$ we obtain

$$\begin{aligned} & I_{\mathrm{FDPB}}(\Delta_1, \tau) \\ \propto\ & \{[1 + n_4 \exp(-2\alpha_1|\tau|)]L_9 + L_{10}\} \\ & + \eta^2 \exp(-2\mathrm{i}\Delta\boldsymbol{k}\cdot\boldsymbol{r})\big\{[1 + n_4 \exp(-2\alpha_2|\tau|)] \\ & \times \chi_M^2 + L_{11}\big\} \\ & + \eta L_8\big\{\exp[\mathrm{i}\Delta\boldsymbol{k}\cdot\boldsymbol{r} - \mathrm{i}(\omega_1 - \omega_2)|\tau|]\chi_B \\ & + \exp[-\mathrm{i}\Delta\boldsymbol{k}\cdot\boldsymbol{r} + \mathrm{i}(\omega_1 - \omega_2)|\tau|]\chi_B^*\big\}. \end{aligned} \tag{12}$$

Here,

$$\begin{aligned} L_9 &= [1 + 3\gamma_M^2/(\gamma_M^2 + \Delta_1^2)]\chi_M^2, \\ L_{10} &= \exp(-2\alpha_1|\tau|)\{[1 + \gamma_M^2/(\gamma_M^2 + \Delta_1^2)] \\ &\quad \times 2\chi_M\chi_T + \chi_T^2\}, \\ L_{11} &= \exp(-2\alpha_2|\tau|)(2\chi_M\chi_T + \chi_T^2), \end{aligned}$$

and $\chi_B = \chi_M + \chi_T + \chi_M\gamma_M/(\gamma_M - \mathrm{i}\Delta_1)$.

Similarly with Raman FDPB, the Rayleigh FDPB shows the femtosecond scale modulation with a different frequency $\omega_1 - \omega_2$ and damping rates α_1 and α_2. Equation (12) for PDM is more insensitive to the intensity fluctuation than that of CFM and is short of decay terms $\exp(-2\alpha_1|\tau|)$ and $\exp(-2\alpha_2|\tau|)$, while Rayleigh FDPB of GAM has the τ-dependent factors $2\exp(-2\alpha_1|\tau|)$ and $2\exp(-2\alpha_2|\tau|)$, which are larger than those of CFM and PDM (see Fig.3). On the other hand, we find that as the Rayleigh-mode detuning $\Delta_1 = 0$, the temporal behavior of the Rayleigh FDPB is symmetric with the maximum of the beat signal at $\tau = 0$ (Fig.3), while as the Raman-mode detuning $\Delta_2 = 0$, the temporal behaviour of the Raman FDPB is asymmetric with the maximum of the beat signal shifted from $\tau = 0$ (Fig.2). It is induced by phase shifts of Raman phase-angle θ_A and Rayleigh phase-angle θ_B, respectively. When $\Delta_1 = \Delta_2 = 0$, we have $\theta_A \neq 0$ and $\theta_B = 0$, as shown in Figs.4(a) and 4(b), respectively.

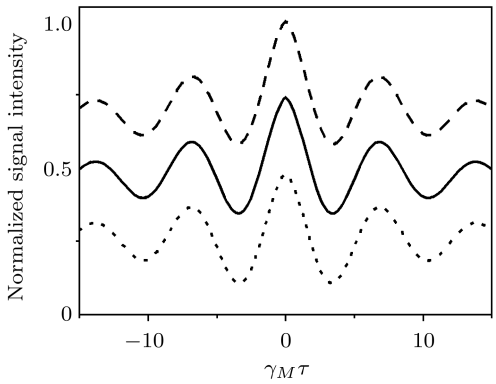


Fig.3. The Rayleigh FDPB signal intensity versus $\gamma_M\tau$ for $\chi_M/\chi_T = 1$, $\gamma_T/\gamma_M = 50$, $\alpha_1/\gamma_M = 0.001$, $\alpha_2/\gamma_M = \alpha_3/\gamma_M = 0.1$, $\Delta_1 = 0$, $r = 0$, $\omega_1/\alpha_1 = 120800$, $\omega_2/\alpha_1 = 119900$ and $\eta = 1$. The three curves represent the signal intensities for CFM (solid curve), GAM (dashed curve), and PDM (dotted curve).

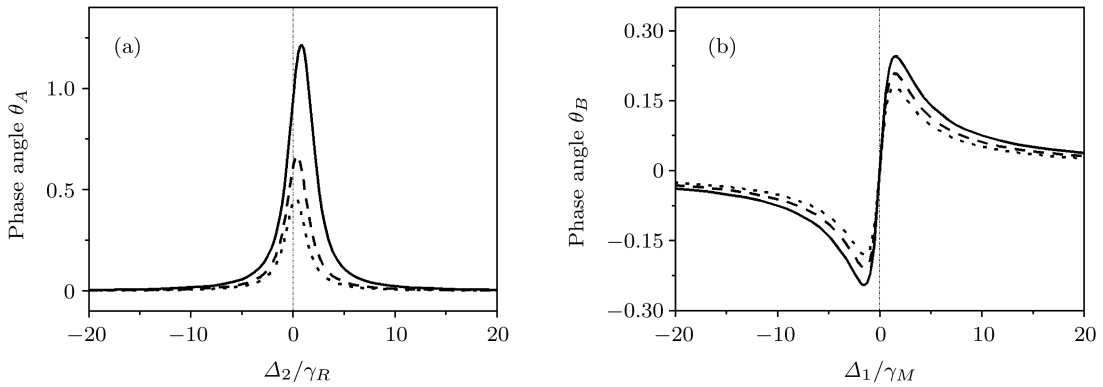


Fig.4. (a) Phase angle θ_A versus frequency detuning Δ_2/γ_R for $\chi_M/\chi_R = \chi_T/\chi_R = 0.9$, $\chi_M/\chi_R = \chi_T/\chi_R = 0.6$, $\chi_M/\chi_R = \chi_T/\chi_R = 0.3$. The three curves represent the variation of θ_A for $\chi_M/\chi_R = \chi_T/\chi_R = 0.3$ (solid curve), that for $\chi_M/\chi_R = \chi_T/\chi_R = 0.6$ (dashed curve), and that for $\chi_M/\chi_R = \chi_T/\chi_R = 0.9$ (dotted curve). (b) Phase angle θ_B versus frequency detuning Δ_1/γ_M for $\gamma_T/\gamma_M = 1 \times 10^{-6}$, $\chi_T/\chi_M = 0.9$, $\chi_T/\chi_M = 0.6$, $\chi_T/\chi_M = 0.3$. The three curves represent variation of θ_B for $\chi_T/\chi_M = 0.3$ (solid curve), that for $\chi_T/\chi_M = 0.6$ (dashed curve), and that for $\chi_T/\chi_M = 0.9$ (dotted curve).

4. The Raman- and Rayleigh-enhanced nonlinear susceptibility

The Raman- and Rayleigh-enhanced nonlinear polarization and the corresponding susceptibility have the relation $P_A = S_2(\boldsymbol{r})\chi_A$ and $P_B = S_1(\boldsymbol{r})\chi_B$. Based on the cross-correlation terms of the Raman FDPB, we can obtain the expression of the Raman-enhanced susceptibility

$$\chi_A = \exp[-(\alpha_1+\alpha_2)\tau]\left(\chi_M + \chi_T + \frac{\mathrm{i}\gamma_R\chi_R}{\alpha_2+\alpha_3+\gamma_R-\mathrm{i}\Delta_2}\right) \tag{13}$$

for $\tau > 0$ and

$$\begin{aligned}\chi_A \;=\; & \exp[(\alpha_1+\alpha_2)\tau]\times(\chi_M+\chi_T)\\ & + \mathrm{i}\gamma_R\chi_R\left\{\frac{\exp[(\alpha_1+\alpha_2)\tau]-\exp[\tau(\alpha_2+\alpha_3+\gamma_R-\mathrm{i}\Delta_2)]}{-\alpha_2+\alpha_3+\gamma_R-\mathrm{i}\Delta_2}+\frac{\exp[\tau(\alpha_2+\alpha_3+\gamma_R-\mathrm{i}\Delta_2)]}{\alpha_2+\alpha_3+\gamma_R-\mathrm{i}\Delta_2}\right\}\end{aligned} \tag{14}$$

for $\tau < 0$. Similarly, the Rayleigh-enhanced susceptibility are

$$\chi_B = \exp[-(\alpha_1+\alpha_2)\tau]\left(\chi_M+\chi_T+\frac{\gamma_M\chi_M}{\alpha_1+\alpha_3-\mathrm{i}\Delta_1+\gamma_M}+\frac{\gamma_T\chi_T}{\alpha_1+\alpha_3-\mathrm{i}\Delta_1+\gamma_T}\right) \tag{15}$$

for $\tau > 0$ and

$$\begin{aligned}\chi_B \;=\; & \exp[(\alpha_1+\alpha_2)\tau]\times(\chi_M+\chi_T)\\ & + \left\{\frac{\exp[(\alpha_1+\alpha_2)\tau]-\exp[\tau(\alpha_2+\alpha_3-\mathrm{i}\Delta_1+\gamma_M)]}{-\alpha_1+\alpha_3-\mathrm{i}\Delta_1+\gamma_M}+\frac{\exp[\tau(\alpha_2+\alpha_3-\mathrm{i}\Delta_1+\gamma_M)]}{\alpha_1+\alpha_3-\mathrm{i}\Delta_1+\gamma_M}\right\}\gamma_M\chi_M\\ & + \left\{\frac{\exp[(\alpha_1+\alpha_2)\tau]-\exp[\tau(\alpha_2+\alpha_3-\mathrm{i}\Delta_1+\gamma_T)]}{-\alpha_1+\alpha_3-\mathrm{i}\Delta_1+\gamma_T}+\frac{\exp[\tau(\alpha_2+\alpha_3-\mathrm{i}\Delta_1+\gamma_T)]}{\alpha_1+\alpha_3-\mathrm{i}\Delta_1+\gamma_T}\right\}\gamma_T\chi_T\end{aligned} \tag{16}$$

for $\tau < 0$. χ_A's (χ_B's) for the three stochastic models (CFM, PDM and GAM) are the same, but those for $\tau > 0$ and $\tau < 0$ are different. χ_A (χ_B) for $\tau < 0$ is more complex due to the interplay between the material and the light responses.

We decompose the nonlinear susceptibilities χ_A and χ_B into a real and an imaginary part, i.e., $\chi_A = \chi'_A + \mathrm{i}\chi''_A$ and $\chi_B = \chi'_B + \mathrm{i}\chi''_B$. On the other hand, χ_A and χ_B can be expressed as $|\chi_A|\exp\mathrm{i}\theta_A = |\chi_A|\cos\theta_A + \mathrm{i}|\chi_A|\sin\theta_A$ with θ_A given by $\theta_A(\Delta_2) = \tan^{-1}(\chi''_A/\chi'_A)$ and $|\chi_B|\exp\mathrm{i}\theta_B = |\chi_B|\cos\theta_B + \mathrm{i}|\chi_B|\sin\theta_B$ with θ_B given by $\theta_B(\Delta_1) = \tan^{-1}(\chi''_B/\chi'_B)$. From Eqs.(13)–(16), we realized that the phase dispersions θ_A and θ_B are greatly modified by the color-locked noisy field with both linewidth α_i and time delay τ for $\tau < 0$, but only with α_i for $\tau > 0$.

Figures 4 and 5 show the phase dispersion of Raman- and Rayleigh-enhanced FWM, including the influence of the color-locked noisy field for $\tau > 0$. In Fig.4(a) the phase angle θ_A shows the absorption-like shape. When χ_M/χ_R and χ_T/χ_R increase, it becomes more symmetrical about $\Delta_2 = 0$, and the value decreases more drastically. On the other hand, in Fig.4(b) we can see that the phase angle θ_B shows a dispersion-like shape and its amplitude decreases as χ_T/χ_M increases. In the cw limit ($\alpha_i = 0$), χ_A's (χ_B's) for $\tau < 0$ and $\tau > 0$ become the same, i.e., $\chi_A = \chi_M + \chi_T - \chi_R\gamma_R/(\Delta_2 + \mathrm{i}\gamma_R)$ and $\chi_B = \chi_M + \chi_T + \chi_M\gamma_M/(\gamma_M - \mathrm{i}\Delta_1) + \chi_T\gamma_T/(\gamma_T - \mathrm{i}\Delta_1)$. $\chi'_A(\Delta_2)$ is neither an odd nor an even function due to χ_M and χ_T terms, and $\chi''_A(\Delta_2)$ is an even function. So θ_A shows the asymmetric absorption-like line shape, while $\theta_B(\Delta_1)$ is an odd function (dispersion-like shape) for even function $\chi'_B(\Delta_1)$ and odd function $\chi''_B(\Delta_1)$. Comparison with the broadband ($\alpha_i/\gamma_M \gg 1$, $\alpha_i/\gamma_T \gg 1$), the dispersion and absorption under narrowband condition are independent of the linewidth α_i and time delay τ, which correspond to the nonmodified nonlinear dispersion and absorption of the material. In Fig.5, θ_A and θ_B decrease and the line shape becomes broad with increasing linewidth, which shows the influence of the field-correlation of the color-locked noisy light. Thus, by virtue of the ultrafast modulation processes within the femtosecond regime, one can optimize the nonlinear susceptibilities and obtain the efficient nonlinear optical signals, which have potential applications in obtaining better nonlinear optical materials and good opt-electronic devices.

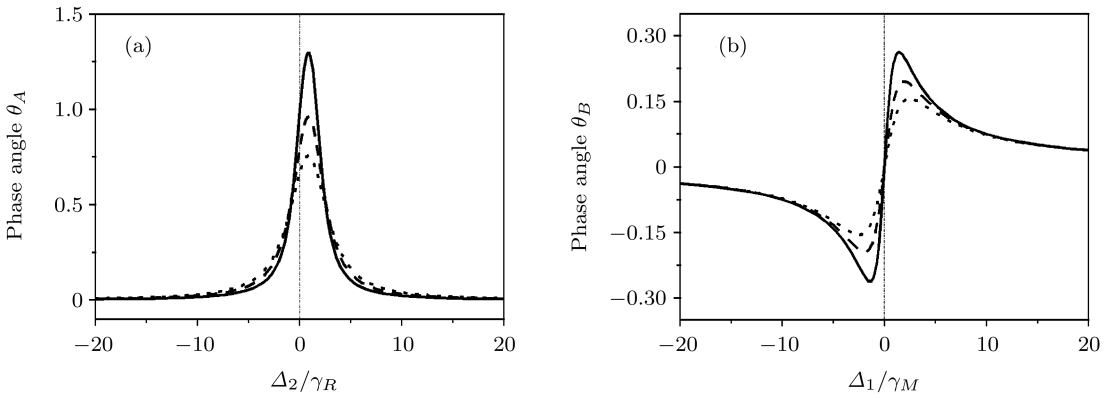


Fig.5. (a) Phase angle θ_A versus frequency detuning Δ_2/γ_R for $\alpha_2/\gamma_R = 1$, $\alpha_2/\gamma_R = 0.5$, $\alpha_2/\gamma_R = 0$. The three curves represent the variations of θ_A at $\alpha_2/\gamma_R = 0$ (solid curve), at $\alpha_2/\gamma_R = 0.5$ (dashed curve), and at $\alpha_2/\gamma_R = 1$ (dotted curve). (b) Phase angle θ_B versus frequency detuning Δ_1/γ_M for $\gamma_T/\gamma_M = 1 \times 10^{-6}$, $\alpha_1/\gamma_M = 1$, $\alpha_1/\gamma_M = 0.5$, $\alpha_1/\gamma_M = 0$. The three curves represent the variations of θ_B at $\alpha_1/\gamma_M = 0$ (solid curve), at $\alpha_1/\gamma_M = 0.5$ (dashed curve), and at $\alpha_1/\gamma_M = 1$ (dotted curve).

5. Heterodyne detection of FDPB

Since optical fields oscillate too quickly for direct detection, they must be measured "in quadrature"-as photons. One of the common measurement techniques, such as FWM measured at its quadrature $I_A = P_A P_A^*$ or $I_B = P_B P_B^*$, yields only absolute value of the nonlinear susceptibility $|\chi_A|^2$ or $|\chi_B|^2$. Thus, all phase information in the nonlinear susceptibility is lost. The second way to achieve quadrature is the phase-sensitive method used for optical heterodyne detection. We introduce another reference FWM

signal designed in frequency and wave vector (Fig.1) to conjugate (go into quadrature) in its complex representation with the new polarization of interest. Both the measured and the reference signals have the same frequency, thus, they interfere directly at the detector and generate FDPB by changing the relative time delay τ between the measured and the reference beams. In other words, the total signal is modulated by the time delay. In the heterodyne case the reference signal is larger than the measured, and the phase information is retained so that one can take a full measure of the complex susceptibility through adjusting the time delay τ.

5.1. Raman FDPB

For the Raman-enhanced FWM signal with polarization P_A, we introduce the reference FWM signal with polarization P_D. Thus the Raman FDPB signal is proportional to the average of the square of the absolute value of $P_A + P_D$ over the random variable of the stochastic process, so the signal intensity $I(\Delta_2, \tau) \propto \langle |P_A + P_D|^2 \rangle = \langle (P_A + P_D)(P_A^* + P_D^*) \rangle = \langle P_A P_A^* \rangle + \langle P_D P_D^* \rangle + \langle P_A P_D^* \rangle + \langle P_D P_A^* \rangle$ contains $5 \times 5 = 25$ different terms in the fourth- and second-order coherence functions of $u_i(t)$ in phase conjugation geometry. In general, the Raman FDPB (at the intensity level) can be viewed as the sum of three contributions: (i) the τ-independent or dependent auto-correlation terms $I_A(\Delta_2, \tau) = \langle P_A P_A^* \rangle$ (i.e., Raman-enhanced FWM) of ω_2 nonresonant molecular-reorientation and thermal gratings, and Δ_2 Raman resonant mode, which includes the $u_2(t)$ fourth-order and the $u_3(t)$ second-order Markovian stochastic correlation functions; (ii) the τ-independent or dependent nonresonant auto-correlation terms $I_D(\tau) = \langle P_D P_D^* \rangle$ of ω_1 molecular-reorientation and thermal gratings, which include $u_1(t)$ fourth-order and $u_3(t)$ second-order Markovian stochastic correlation functions; (iii) the τ-dependent cross-correlation terms $I_{A,D}(\Delta_2, \tau) = \langle P_A P_D^* \rangle + \langle P_D P_A^* \rangle$ between Raman-enhanced FWM and NDFWM processes, which include $u_1(t)$, $u_2(t)$ and $u_3(t)$ second-order Markovian stochastic correlation functions. Different Markovian stochastic models of the laser field only affect the fourth-, not the second-order correlation functions. Therefore, the cross-correlation terms are the same for the three Markovian stochastic models. Furthermore, by virtue of the cross-correlation term $I_{A,D}(\Delta_2, \tau)$ we can obtain the third-order susceptibilities for the Raman-enhanced FWM $\chi_A = \chi_M + \chi_T - \chi_R \gamma_R / [\Delta_2 + \mathrm{i}(\alpha_2 + \alpha_3 + \gamma_R)]$ and for the reference NDFWM $\chi_D = \chi_M + \chi_T$ theoretically. The real and imaginary parts of χ_A are respectively odd and even functions, i.e., $\chi_A' = \chi_M + \chi_T - \chi_R \gamma_R \Delta_2 / [\Delta_2^2 + (\alpha_2 + \alpha_3 + \gamma_R)^2]$ and $\chi_A'' = \chi_R \gamma_R (\alpha_2 + \alpha_3 + \gamma_R) / [\Delta_2^2 + (\alpha_2 + \alpha_3 + \gamma_R)^2]$.

In heterodyne detection, we assume $I_D(\tau) \gg I_A(\Delta_2, \tau)$ at intensity level, in other words, we let $\eta \ll 1$, thus we have $I \propto I_D(\tau) + I_{A,D}(\Delta_2, \tau)$. For simplicity, in the limit of γ_R, $\gamma_M \gg \alpha_1$, α_2, $\alpha_3 \gg \gamma_T$ and based on the chaotic, phase-diffusion and real Gaussian fields, we have their Raman FDPB signals, respectively, i.e.,

$$\begin{aligned} & I_{\mathrm{FDPB}}(\Delta_2, \tau) \\ \propto & \left\{ [1 + n_4 \exp(-2\alpha_1 |\tau|)] \chi_M^2 + L_7 \right\} \\ & + \eta L_8 \Big\{ \exp[\mathrm{i} \Delta \boldsymbol{k} \cdot \boldsymbol{r} - \mathrm{i}(\omega_1 - \omega_2)|\tau|] \chi_A^* \\ & + \exp[-\mathrm{i} \Delta \boldsymbol{k} \cdot \boldsymbol{r} + \mathrm{i}(\omega_1 - \omega_2)|\tau|] \chi_A \Big\}. \end{aligned} \tag{17}$$

We express χ_A as $|\chi_A| \exp(\mathrm{i}\theta_A) = |\chi_A| \cos\theta_A + \mathrm{i} |\chi_A| \sin\theta_A$ with variation of θ_A shown in Figs.4(a) and 5(a). Therefore, we have

$$\begin{aligned} & I_{\mathrm{FDPB}}(\Delta_2, \tau) \\ \propto & I_D(\tau) + 2 L_8 \eta |\chi_A| \cos[-\Delta \boldsymbol{k} \cdot \boldsymbol{r} \\ & + (\omega_1 - \omega_2)|\tau| + \theta_A]. \end{aligned} \tag{18}$$

Equation (18) indicates that the reference FWM signal $I_D(\tau)$ and the factor $2L_8\eta$ are independent of Δ_2, while the heterodyne signal is modulated with a sum-frequency $\omega_1 - \omega_2$ as τ is varied; in addition, the phase of the oscillation depends on the phase θ_A of the measured third-order susceptibility χ_A. If we adjust the time delay τ such that $-\Delta \boldsymbol{k} \cdot \boldsymbol{r} + (\omega_1 - \omega_2)|\tau| = 2n\pi$, then

$$\begin{aligned} & I_{\mathrm{FDPB}}(\Delta_2, \tau) \\ \propto & I_D(\tau) + 2 L_8 \eta |\chi_A| \cos\theta_A \propto I_D(\tau) \\ & + 2 L_4 \eta \chi_A'. \end{aligned} \tag{19}$$

However, if $-\Delta \boldsymbol{k} \cdot \boldsymbol{r} + (\omega_1 - \omega_2)|\tau| = (2n - 1/2)\pi$, we have

$$\begin{aligned} & I_{\mathrm{FDPB}}(\Delta_2, \tau) \\ \propto & I_D(\tau) + 2 L_8 \eta |\chi_A| \sin\theta_A \propto I_D(\tau) \\ & + 2 L_4 \eta \chi_A''. \end{aligned} \tag{20}$$

In other words, by changing the time delay τ between beams 1 and 2 we can obtain the real and the imaginary parts of the Raman-enhanced susceptibility χ_A.

Figure 6 shows the heterodyne detection spectra versus Δ_2/γ_R of the Raman FDPB. We can see that the spectra have the profile of the real and imaginary parts of the Raman resonance with comparable backgrounds. On the other hand, in Fig.6 the spectra of CFM, PDM and GAM are the same as those of the cw beam. However, the background of the three Markovian models is smaller than that of the cw beam due to the phase fluctuation.

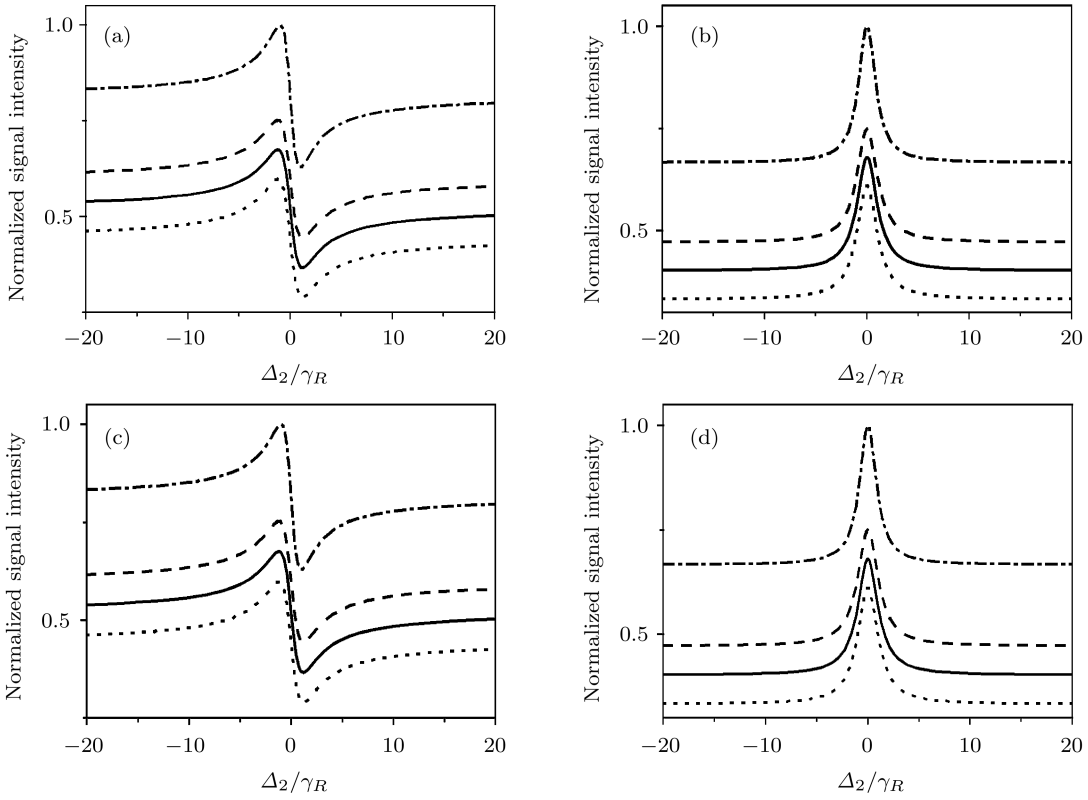


Fig.6. The heterodyne detection spectra versus Δ_2/γ_R of Raman FDPB for $\chi_M/\chi_R = 0.1$, $\gamma_M/\alpha_1 = \gamma_R/\alpha_1 = 10$, $\chi_T/\chi_R = 0.1$, $\gamma_T/\alpha_1 = 1 \times 10^{-5}$, $\alpha_2/\alpha_1 = \alpha_3/\alpha_1 = 1$, $\Delta\boldsymbol{k} = 0$; (a) $\tau = (2\pi)/(\omega_1 - \omega_2) > 0$ and (c) $\tau = (-2\pi)/(\omega_1 - \omega_2) < 0$ for $\mathrm{Re}\,\chi_A$, (b) $\tau = (1.5\pi)/(\omega_1 - \omega_2) > 0$ and (d) $\tau = (-1.5\pi)/(\omega_1 - \omega_2) < 0$ for $\mathrm{Im}\,\chi_A$ with $\omega_1/\alpha_1 = 127450$, $\omega_2/\alpha_1 = 119924$.

5.2. Rayleigh FDPB

For the Rayleigh-enhanced FWM signal with polarization P_B, we introduce the reference FWM signal with polarization P_C. Thus the Rayleigh FDPB signal is proportional to the average of the square of absolute value of $P_B + P_C$, so the signal intensity $I(\Delta_1, \tau) \propto \langle |P_B + P_C|^2 \rangle = \langle (P_B + P_C)(P_B^* + P_C^*) \rangle$ contains $6 \times 6 = 36$ different terms where $I_B(\Delta_1, \tau) = \langle P_B P_B^* \rangle$ and $I_C(\tau) = \langle P_C P_C^* \rangle$ include the $u_1(t)$ and the $u_2(t)$ fourh-order Markovian stochastic correlation functions, respectively; while $I_{B,C}(\Delta_1, \tau) = \langle P_B P_C^* \rangle + \langle P_B P_C^* \rangle$ includes $u_i(t)$ second-order Markovian stochastic correlation functions. We know that different Markovian stochastic models of the laser field only affect the fourth-, not the second-order correlation functions. Therefore, the cross-correlation terms $I_{B,C}(\Delta_1, \tau)$ are the same for the three Markovian stochastic models, from which we can obtain the third-order susceptibilities for the Rayleigh-enhanced FWM $\chi_B = \chi_M + \chi_T + \chi_M\gamma_M/[(\alpha_1 + \alpha_3 + \gamma_M) - \mathrm{i}\Delta_1] + \chi_T\gamma_T/[(\alpha_1 + \alpha_3 + \gamma_T) - \mathrm{i}\Delta_1]$ and for the reference NDFWM $\chi_C = \chi_M + \chi_T$ theoretically. The real and imaginary parts of χ_B are respectively even and odd functions, i.e.,

$$\begin{aligned}
&\chi_B' \\
&= \chi_M + \chi_T \\
&\quad + \gamma_M(\alpha_1 + \alpha_3 + \gamma_M)\chi_M/[(\alpha_1 + \alpha_3 + \gamma_M)^2 + \Delta_1^2] \\
&\quad + \gamma_T(\alpha_1 + \alpha_3 + \gamma_T)\chi_T/[(\alpha_1 + \alpha_3 + \gamma_T)^2 + \Delta_1^2]
\end{aligned}$$

and

$$\chi''_B = \chi_M\gamma_M\Delta_1/[(\alpha_1+\alpha_3+\gamma_M)^2+\Delta_1^2] + \chi_T\gamma_T\Delta_1/[(\alpha_1+\alpha_3+\gamma_T)^2+\Delta_1^2].$$

In heterodyne detection, we assume $I_C(\tau) \gg I_B(\Delta_1,\tau)$ at the intensity level, in other words, we let $\eta \gg 1$, so that we have $I(\Delta_1,\tau) \propto I_C(\tau)+I_{B,C}(\Delta_1,\tau)$. Under the condition of $\gamma_M \gg \alpha_1,\alpha_2,\alpha_3 \gg \gamma_T$, we have the Rayleigh FDPB signals for the three Markovian models, i.e. ,

$$\begin{aligned} &I_{\mathrm{FDPB}}(\Delta_1,\tau) \\ &\propto \eta^2\exp(-2\mathrm{i}\Delta\boldsymbol{k}\cdot\boldsymbol{r})\{[1+n_4\exp(-2\alpha_2|\tau|)]\chi_M^2 \\ &\quad + L_{11}\} + \eta L_8\Big\{\exp[\mathrm{i}\Delta\boldsymbol{k}\cdot\boldsymbol{r}-\mathrm{i}(\omega_1-\omega_2)|\tau|]\chi_B \\ &\quad + \exp[-\mathrm{i}\Delta\boldsymbol{k}\cdot\boldsymbol{r}+\mathrm{i}(\omega_1-\omega_2)|\tau|]\chi_B^*\Big\}. \end{aligned} \tag{21}$$

We express χ_B as $|\chi_B|\exp(\mathrm{i}\theta_B) = |\chi_B|\cos\theta_B + \mathrm{i}\,|\chi_B|\sin\theta_B$, with θ_B expressed as in Figs.4(b) and 5(b). From Eq.(21) we have

$$\begin{aligned} I_{\mathrm{FDPB}}(\Delta_1,\tau) &\propto I_C(\tau)+2L_8\eta|\chi_B|\cos[\Delta\boldsymbol{k}\cdot\boldsymbol{r} \\ &\quad -(\omega_1-\omega_2)|\tau|+\theta_B]. \end{aligned} \tag{22}$$

Equation (22) indicates that the reference FWM signal $I_C(\tau)$ and the factor $2L_8\eta$ are independent of Δ_1. The heterodyne signal is modulated with a sum-frequency $\omega_1-\omega_2$ as τ is varied. In addition, the phase of the oscillation depends on the phase θ_B of the measured third-order susceptibility χ_B. If we adjust the time delay τ such that $\Delta\boldsymbol{k}\cdot\boldsymbol{r}-(\omega_1-\omega_2)|\tau| = 2n\pi$, then

$$\begin{aligned} I_{\mathrm{FDPB}}(\Delta_1,\tau) &\propto I_C(\tau)+2L_8\eta|\chi_B|\cos\theta_B \\ &\propto I_C+2L_4\eta\chi'_B. \end{aligned} \tag{23}$$

However, if $\Delta\boldsymbol{k}\cdot\boldsymbol{r}-(\omega_1-\omega_2)|\tau| = (2n-1/2)\pi$, we have

$$\begin{aligned} I_{\mathrm{FDPB}}(\Delta_1,\tau) &\propto I_C(\tau)+2L_8\eta|\chi_B|\sin\theta_B \\ &\propto I_C(\tau)+2L_4\eta\chi''_B. \end{aligned} \tag{24}$$

In other words, by changing the time delay τ between beams 1 and 2 we can obtain the real and the imaginary parts of the Rayleigh-enhanced susceptibility χ_B.

Figure 7 shows the heterodyne detection spectra versus Δ_1/γ_R of the Rayleigh FDPB. We can see that

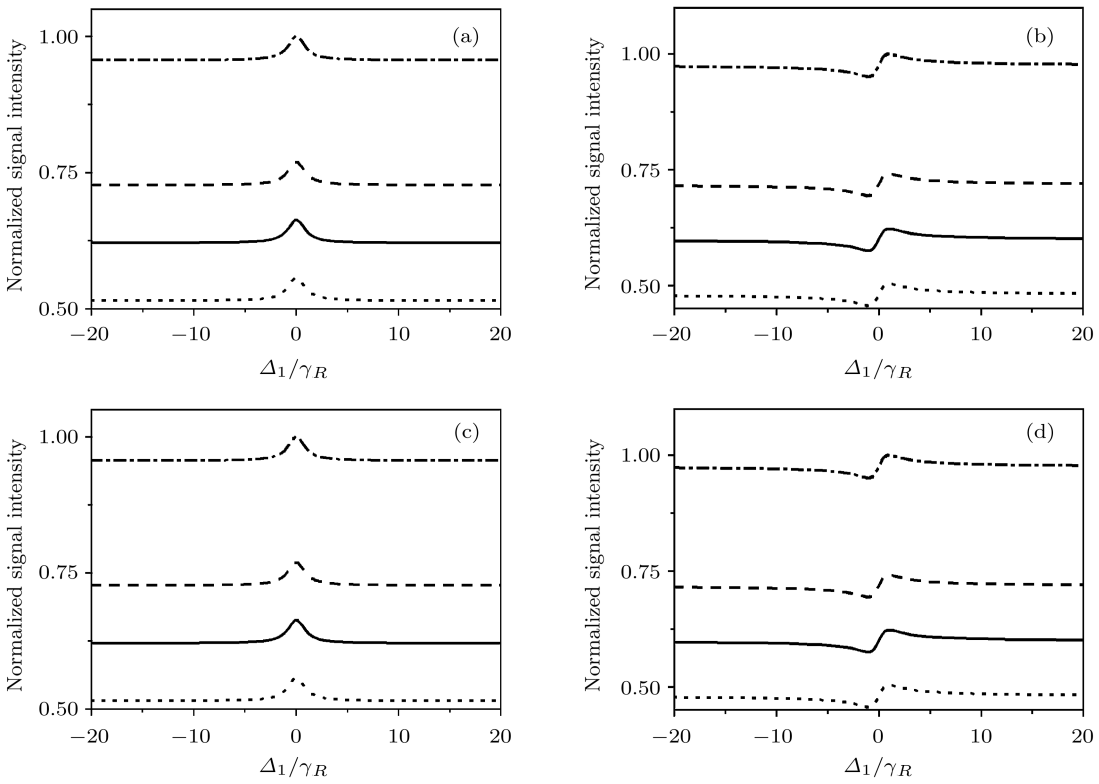


Fig.7. The heterodyne detection spectra versus Δ_1/γ_R of Rayleigh FDPB for $\chi_M/\chi_T = 1$, $\gamma_M/\alpha_1 = 100$, $\gamma_T/\alpha_1 = 1\times10^{-5}$, $\alpha_2/\alpha_1 = \alpha_3/\alpha_1 = 1$, $\Delta\boldsymbol{k} = 0$; (a) $\tau = (2\pi)/(\omega_1-\omega_2) > 0$ and (c) $\tau = (-2\pi)/(\omega_1-\omega_2) < 0$ for $\mathrm{Re}\,\chi_B$, (b) $\tau = (1.5\pi)/(\omega_1-\omega_2) > 0$ and (d) $\tau = (-1.5\pi)/(\omega_1-\omega_2) < 0$ for $\mathrm{Im}\,\chi_B$, with $\omega_1/\alpha_1 = 120800$, $\omega_2/\alpha_1 = 119900$.

the spectra exhibit the profiles of the real and imaginary parts of the Rayleigh resonance with comparable backgrounds. It is clear that the curves represent the even function for the real part and the odd function for the imaginary part of χ_B, which is just opposite to those of the Raman-enhanced susceptibility χ_A (Fig.6). On the other hand, similarly, for the heterodyne signal of Rayleigh FDPB the spectra of cw beams are the same as those of CFM, PDM and GAM. However, the spectra of cw beams have the largest background while the spectra of PDM have the smallest background due to the absence of the amplitude fluctuation.

5.3. The mixing of Raman and Rayleigh

In fact, the conditions for exciting Raman and Rayleigh modes can be satisfied ($\Delta_1 = \Delta_2 = \Delta_1' - \Omega_R \approx 0$) in one experiment system simultaneously and the Raman- and Rayleigh-enhanced FWM's are mixed and interfere with each other. Each of them can be considered as the reference signal of the other. For the heterodyne detection we have the polarization beat signal $I(\Delta_1, \Delta_2, \tau) \propto \langle (P_A + P_B)(P_A^* + P_B^*) \rangle$ for studying the phase dispersion of the Raman- or Rayleigh-enhanced third-order susceptibilities χ_A and χ_B. For example, the picture shows the FDPB spectra versus Δ_1/γ_R and Δ_2/γ_R in the case of $I_A(\Delta_2, \tau) \ll I_B(\Delta_1, \tau)$. As the value of Δ_1/γ_R satisfies the condition of $-\Delta\boldsymbol{k}\cdot\boldsymbol{r} + (\omega_1 - \omega_2)|\tau| - \theta_B = 2n\pi$, the spectra versus Δ_2/γ_R showing the real part of χ_A have a dispersive shape (Fig.8.).

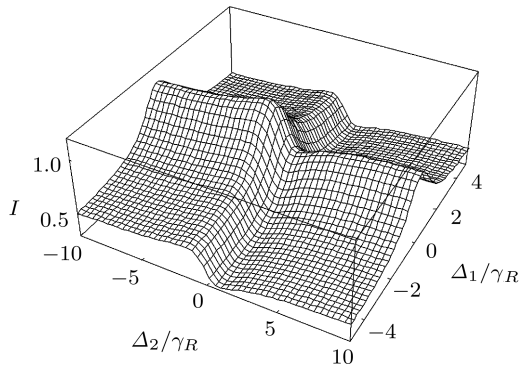


Fig.8. The heterodyne detection spectra (CFM) versus Δ_1/γ_R and Δ_2/γ_R of the coexisting Raman and Rayleigh FDPB in the case of $I_A(\Delta_2, \tau) \ll I_B(\Delta_1, \tau)$ for $\chi_M/\chi_R = 0.1$, $\gamma_M/\alpha_1 = \gamma_R/\alpha_1 = 10$, $\chi_T/\chi_R = 0.1$, $\gamma_T/\alpha_1 = 1 \times 10^{-5}$, $\alpha_2/\alpha_1 = \alpha_3/\alpha_1 = 1$, $\Delta\boldsymbol{k} = 0$, $\tau = (\theta_B - 2\pi)/(\omega_1 - \omega_2)$ for $\mathrm{Re}\,\chi_B$.

6. Discussion and conclusion

Based on the three stochastic models, the subtle Markovian field-correlation effects have been investigated in Raman- and Rayleigh-enhanced FWM, homodyne- and heterodyne-detected FDPB. All of these can be understood in the time and frequency domains. In this paper we have employed the FDPB to obtain the real and the imaginary parts of the Raman and Rayleigh resonances based on the polarization interference between normal FWM and Raman- or Rayleigh-enhanced FWM processes, even between Raman- and Rayleigh-enhanced FWM processes. Specifically, since Raman- and Rayleigh-enhanced FWM signals propagate along the same optical path, in the heterodyne detection of FDPB, we purposely introduce them as the reference signal for each other. Our method is based on the polarization interference between two competitive Raman- and Rayleigh-enhanced FWM processes. The detunings Δ_1 and Δ_2 control the intensity and phase angle of Rayleigh- and Raman-enhanced susceptibilities χ_B and χ_A, respectively. We need scanning one detuning to show the phase dispersion of χ_B or χ_A with proper time delay, while the other one can be obtained only by changing the reference background. If the change of Δ_1 or Δ_2 is large enough, the value of θ_B or θ_A will equal zero, and the coexisting Raman and Rayleigh FDPB will be converted into the pure Raman or Rayleigh FDPB.

In conclusion, based on color-locking noisy field correlation in the three Markovian stochastic models, phase dispersions of the Raman- and Rayleigh-enhanced four-wave mixing (FWM) have been investigated. The phase dispersions θ_A and θ_B are greatly modified by the color-locked noisy field with both linewidth α_i and time delay τ for $\tau < 0$, but only α_i for $\tau > 0$. Moreover, the results under narrowband condition are close to those of the nonmodified nonlinear dispersion and absorption of the material. In addition, based on the three stochastic models, homodyne (quadratic) and heterodyne (linear) detection of the Raman FDPB, the Rayleigh FDPB and the coexisting Raman and Rayleigh FDPB have also been investigated, separately. From the heterodyne detected FDPB, we can obtain the characteristics of the dispersion and absorption for the resonant Raman- and Rayleigh-enhanced FWM, and they help us to understand and optimize the nonlinear susceptibilities

and the generated high-order nonlinear optical signals. These results have potential applications in achieving better nonlinear optical materials and good opt-electronic devices.

References

[1] Ulness D J 2003 *J. Phys. Chem.* A **107** 8111

[2] Zhang Y P, Gan C L, Song J P, Yu X J, Ma R Q, Ge H, Li C S and Lu K Q 2005 *J. Opt. Soc. Am.* B **22** 694

[3] Zhang Y P, Gan C L, Li L, Ma R Q, Song J P, Jiang T, Yu X J, Li C S, Ge H and Lu K Q 2005 *Phys. Rev.* A **72** 013812

[4] Gan C L, Nie Z Q, Li L, Shen L J, Zhang Y P, Song J P, Li Y Y, Zhang X C and Lu K Q 2007 *Chin. Phys.* **16** 3407

[5] Fu P M, Jiang Q, Mi X and Yu Z H 2002 *Phys. Rev. Lett.* **88** 113902

[6] DeBeer D, Usadi E and Hartmann S R 1988 *Phys. Rev. Lett.* **60** 1262

[7] Zhang Y P, Brown A W and Xiao M 2007 *Phys. Rev. Lett.* **99** 123603

[8] Zhang Y P, Brown A W and Xiao M 2007 *Opt. Lett.* **32** 091120

[9] Wu Y, Saldana J and Zhu Y F 2003 *Phys. Rev.* A **67** 013811

[10] Wu Y and Deng L 2004 *Opt. Lett.* **29** 1144

[11] Wang H, Goorskey D and Xiao M 2001 *Phys. Rev. Lett.* **87** 073601

[12] Wu H B, Chang H, Ma J, Xie C D and Wang H 2005 *Acta Phys. Sin.* **54** 8 (in Chinese)